



# Deep reactive ion etching of silicon using non-ICP-based equipment

Zaifa Du<sup>1</sup> · Junyang Nie<sup>2,3,4</sup> · Dianlun Li<sup>2,3</sup> · Weiling Guo<sup>1</sup> · Qun Yan<sup>2,3</sup> · Le Wang<sup>1</sup> · Tailiang Guo<sup>2,3</sup> · Jie Sun<sup>2,3</sup>

Received: 17 April 2020 / Accepted: 15 June 2020 / Published online: 19 June 2020  
© Springer-Verlag GmbH Germany, part of Springer Nature 2020

## Abstract

Deep reactive ion etching (DRIE) technology is one of the most important technologies in the processing of microelectronic devices and microelectromechanical system. As a necessary process in semiconductor integration, it has been widely studied in the past decades. It is known that the traditional DRIE process typically uses a plasma etching reactor equipped with inductively coupled plasma (ICP) sources to generate a high-density plasma so as to achieve high aspect ratio trenches with relatively small roughness. A cryogenic temperature control unit is typically employed as well. Here, however, we use a parallel plate RIE with rather simple structure, which is not usually used for DRIE, to obtain high aspect ratio silicon etching. With no ICP sources and no sophisticated temperature control unit, the system and experiment are now much more cost effective. Through the optimization of the processing, the etching rate of silicon can reach 440 nm/min. Finally, a 45 μm deep trench is etched in silicon with good perpendicularity. This method will greatly reduce the equipment related cost, especially for those applications that do not have extremely stringent requirement on the final etching accuracy.

**Keywords** Deep reactive ion etching · Silicon · Etching rate · Inductively coupled plasma

## 1 Introduction

At present, microelectronic and optoelectronic devices are aggressively becoming smaller and more precise. For many devices, their sizes can be as small as micro- or even nano-scale. To etch and fabricate patterns in those devices on electronic chips, it seems inevitable to apply advanced etching

technology. Wet etching technology, in the case of difficult control accuracy, would easily cause damages to the device structures and fail to meet the expected requirements, which makes the alternative dry etching particularly important in the fabrication of micro- and nanodevice structures. Reactive ion etching (RIE) has good selectivity, clear anisotropy and good controllability of etching precision, which makes it widely used in microelectronics and optoelectronics processing [1–5]. Since 1990s, the demand on the so-called deep reactive ion etching (DRIE) has become higher than ever. That is etching trenches in semiconductors with high aspect ratio. In the past two decades or so, there have been two major companies whose dry etching machines occupy the DRIE market: Alcatel and Surface Technology Systems (STS). Those machines have somewhat similar structures which employ inductively coupled plasma (ICP) sources to generate high-density plasma and provide the basis for relatively high silicon etching rates. They are also equipped with a cryogenically cooled wafer chuck that can accurately control the temperature, typically in the range of –140–0 °C [6, 7]. That deep etching process is commonly referred as the “Bosch” process, in which it passivates the sidewall to achieve a good morphology. It uses two sources so that the generation of plasma and the application of bias can be controlled separately. During the etching, first, usually with a

---

Zaifa Du and Junyang Nie contributed equally.

---

✉ Jie Sun  
jie.sun@fzu.edu.cn  
Weiling Guo  
guoweiling@bjut.edu.cn

<sup>1</sup> Laboratory of Optoelectronic Technology, Beijing University of Technology, Beijing 100124, China

<sup>2</sup> National and Local Joint Engineering Laboratory for Flat Panel Display Technology, Fuzhou University, and Fujian Science & Technology Innovation Laboratory for Optoelectronic Information of China, Fuzhou 350108, China

<sup>3</sup> Fujian Science & Technology Innovation Laboratory for Optoelectronic Information of China, Fuzhou 350100, China

<sup>4</sup> Faculty of Electronic and Information Engineering, Xi’an Jiaotong University, Xi’an 710049, China

c-C<sub>4</sub>F<sub>8</sub> based chemistry, it coats the surfaces with a Teflon-like polymer [8]. Second, often with an SF<sub>6</sub>-based chemistry, it removes the polymer on horizontal surfaces and etches the exposed silicon [9]. The cycling of alternating passivation and etching steps facilitates the formation of high aspect ratio silicon features at a relatively high etching rate.

In this paper, however, we use a simpler and relatively inexpensive parallel plate-based RIE system to accomplish deep silicon etching. This type of equipment is rather common in ordinary structure etching but has thus far been overlooked in deep silicon etching. We show that by optimizing the parameters of the etching process (including the etching gas flow, the type of gases, the power applied during the experiment, and the processing time), a silicon trench as deep as 45 μm with good morphology can be obtained using metal etching mask. Apart from the fact that our etcher only has one simple radio frequency (RF) plasma source with much lower power, another major difference between our DRIE and the standard ICP-based DRIE is that we do not employ any sophisticated cryogenic system to control the temperature, which has been crucial to the traditional DRIE. The results show that after optimization, at least in some cases, DRIE of silicon can be accomplished with this kind of simpler etching machine. This is especially important for those applications (such as microscopic mold making, roll-to-roll printing template, etc.) that have relatively loose requirements on the final etching results, but rather pursue to use cost-effective facilities. It renders a number of deep etching processes less dependent on the Bosch technique. Finally, we note that in literature this type of non-ICP-based DRIE of silicon is very rare, which makes this method worthy of research and promotion.

## 2 DRIE etching principle and equipment structure

### 2.1 Etching principle

There are two functions throughout the entire DRIE process, which are physical bombardment and chemical etching. When the injected gases are dissociated into reactive particles, some positive ions are accelerated under the action of bias electric field and bombard the surface of the etched sample vertically. Si–Si bonds can break under the bombardment of positive ions, resulting in more dangling bonds. These dangling bonds combine with the particles diffused from the plasma layer, which makes the radicals firmly adsorb on the sample surface and react with the sample [9]. Because they are volatile, the generated product particles are desorbed at the substrate temperature, diffused to troposphere, and discharged by the extraction system [10]. Taking

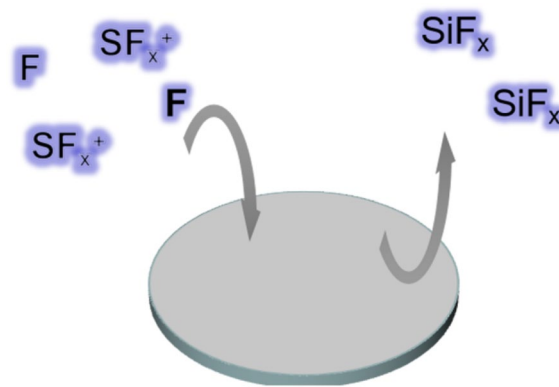


**Fig. 1** Schematic diagram of the F based gas etching reaction of silicon

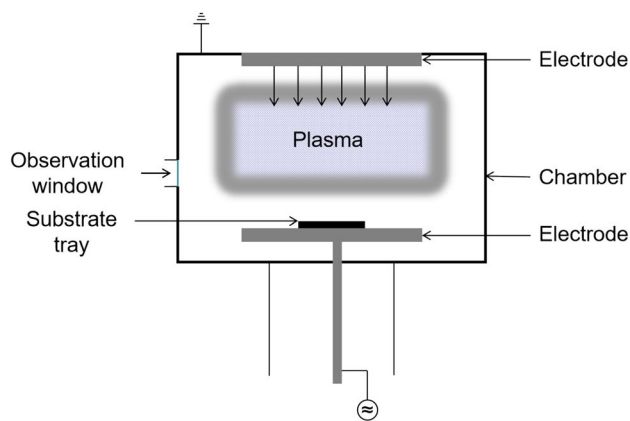


**Fig. 2** Equipment structure of the RIE used in this study

the SF<sub>6</sub> based etching of silicon as an example, the reaction process is schematically shown in Fig. 1.

The corresponding chemical reaction formulas are shown as follows [11]:



### 2.2 Equipment structure

The Tailong RIE-150A etching machine developed by the Institute of Microelectronics, Chinese Academy of Sciences, is used in this experiment. Its structure is shown in Fig. 2.

Almost every commercial ICP-based equipment that is used for standard DRIE involves a sophisticated temperature control system based on liquid helium or liquid nitrogen. In our simpler system, however, there is only a water cooling function used during the etching, which is certainly not intended for cooling towards cryogenic temperatures. This

notwithstanding, as shown below, our system can ensure the Si deep dry etching experiment to be conducted effectively.

### 3 Experiments and data analysis

#### 3.1 Experimental methods and procedures

In this experiment, intrinsic silicon wafers purchased from Suzhou Research Materials Co., Ltd. were used. After dicing, they were placed in a beaker and boiled with acetone and ethanol, respectively. This process was repeated twice. Then, they were rinsed for 30 times with deionized water and blown dry. Afterwards, they were put onto the hot plate and heated for 5 min. After patterning using a photolithography machine, Ti/Ni with a thickness of 10 nm/800 nm was deposited on the Si wafers as an etching mask. A sputtering machine was used for the mask deposition to ensure good adhesion between the masking layer and the silicon. After the deposition, standard lift-off process was performed to obtain the desired pattern. Subsequently, the as-prepared samples were etched using the RIE equipment described above. By changing the experimental conditions including the RF power, the gas flow rates, the initial etched depth, etc., their influences on the Si etching rate were carefully studied and analyzed. To avoid any ambiguities, when studying the effect of a certain parameter on the etching rate, other items remained literally unchanged. The Si etching depths were determined using scanning electron microscopy (SEM).

#### 3.2 Effect of different RF powers on the etching rate

SF<sub>6</sub> is used as the etching gas. The gas flow rate is 80 sccm, the chamber pressure is 4.13 Pa, and the etching time is 10 min. The RF power is changed, and the influence of different RF power on the etching rate is investigated.

Figure 3 shows that as the RF power increases, the etching rate of the silicon greatly increases. This is because at increasing RF power, the particles that are existing in the supplied gases are enhanced in scattering, namely the collision becomes more severe [12]. In this way, the numbers of ions, electrons, and radicals are increased, and the chemical etching activity is naturally enhanced. Furthermore, the increasing RF power enhances the electric field between the two poles, which makes the surface of silicon be physically bombarded more severely by those positive ions. However, this effect is relatively minor because the ion energy is only increased moderately since it is mainly determined by the direct current (DC) voltage. Anyway, it does provide somewhat more active sites, which also accelerates the chemical reaction process [9]. According to the slope of the curve, however, we speculate that when the RF power reaches a

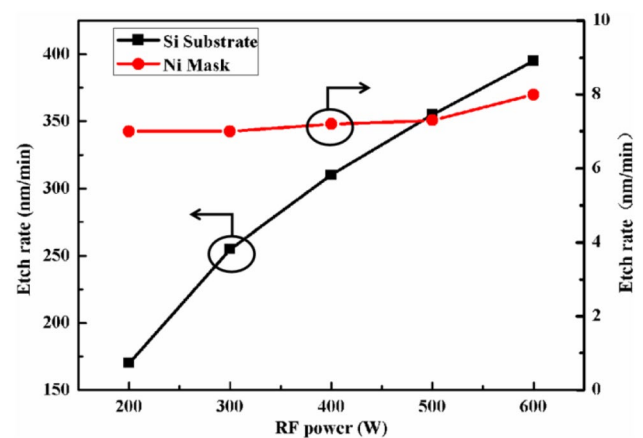


Fig. 3 SF<sub>6</sub> etching rate diagram of the Si (left) and the Ni (right) plotted with changing power

certain high level, the etching rate would not continue to increase, which is because the molecules that are sources of decomposition and ionization are exhausted [13]. It can be seen from Fig. 3 that when the RF power rises, the etching of the masking layer material (Ni) is strengthened only slightly. The etching rate is rather stable between 7 and 8 nm/min, which is a much smaller value compared to the rate of Si etching. This is because the Ni mask is mainly etched by the physical bombardment since fluorine does not chemically react with Ni. When the RF power is increased, as mentioned before, the ion energy is increased only a little and, therefore, the Ni etch rate increases just slightly. It indicates that the nickel layer is indeed a good mask, which is quite resistant to both the chemical and the physical etching in the machine, even at increasing RF powers. In Fig. 3, the best Si to Ni selectivity of 49:1 can be reached when the RF power is 500 W. The etching rate of the Si substrate can be ensured, and the masking layer can be well preserved, which is the optimal working condition in our experiments.

#### 3.3 Effect of different kinds of etching gases and flow rates on the etching rate

Different types of etching gases with different ratios of the mixture are investigated in terms of the effect on the Si etching rate. Figure 4a–c show the effect on the etching rate for SF<sub>6</sub>, SF<sub>6</sub>/CHF<sub>3</sub> and SF<sub>6</sub>/O<sub>2</sub> gases at different ratios. The experiments above are carried out under the condition of 500 W RF power. The etching time for every sample in Fig. 4 is fixed at 20 min.

As shown in Fig. 4a, the etching rate of the Si sample increases while the flow rate of the SF<sub>6</sub> gas source increases (No other gas species is added during this experiment). This is straightforward to understand, because the number of reactive ions increases, and the reaction with the surface

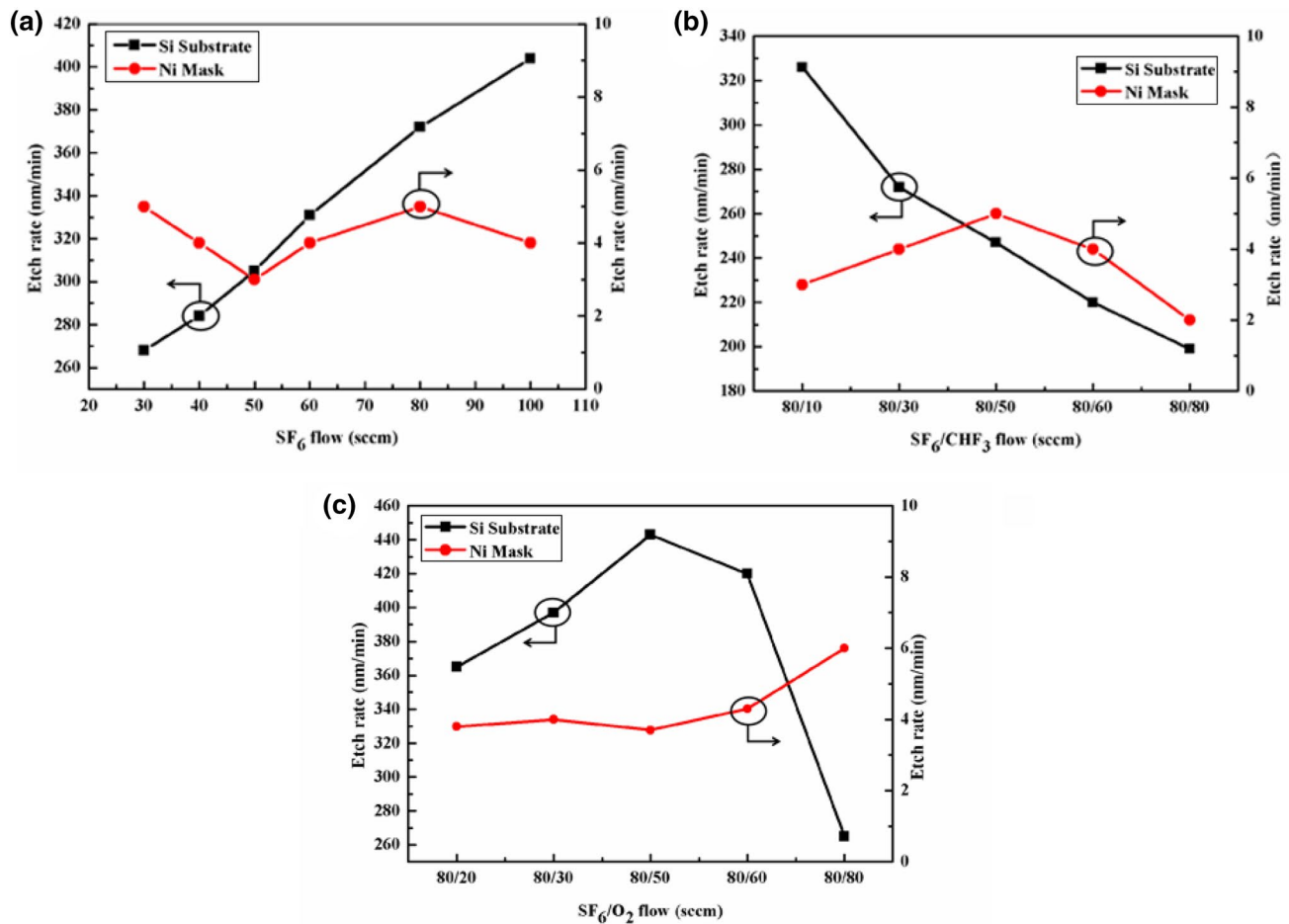


**Fig. 4** a Etching rate diagram with different SF<sub>6</sub> gas flow rates; b etching rate diagram with different flow rates and ratios of the SF<sub>6</sub>/CHF<sub>3</sub> gas mixture; c Etching rate diagram with different SF<sub>6</sub>/O<sub>2</sub> flow

rates and ratios of the gas mixture (the curve with black blocks is the Si etching rate and the curve with red circles is for the etching of the Ni mask)

of the etched sample is hence accelerated. The physical bombardment is also more intensive. Those effects naturally result in the increase of the etching rate. In contrast, the etching rate of the mask layer is not sensitive to the change of the gas source flow rate, and the etching rate is fluctuating within  $4 \pm 1$  nm/min. The change of the gas flow has little effect on the etching of the masking layer, implying a superior dry etching selectivity of Si to Ni, in agreement with the conclusion reached in the earlier discussion.

It is known that CHF<sub>3</sub> can also be used for silicon etching [14]. Therefore, we have mixed SF<sub>6</sub> with CHF<sub>3</sub> to see if there are any combined effects. Figure 4b shows the effect of different SF<sub>6</sub>/CHF<sub>3</sub> gas flows and ratios on the etching rate. As the amount of incorporated CHF<sub>3</sub> increases, the etching rate of the substrate material decreases. In the process of silicon etching, F element plays a major role. When adding CHF<sub>3</sub> into SF<sub>6</sub>, because the total flow increases, it actually increases the amount of F (dissociated from both SF<sub>6</sub> and CHF<sub>3</sub>). At a first glance, it seems counterintuitive why the

etching rate still gets down. In fact, CF<sub>2</sub> radicals, as products from the CHF<sub>3</sub> plasma, are generated, which will form a C<sub>x</sub>F<sub>y</sub> blocking layer on the Si surface [10, 15, 16]. That is the dominant reason for slowing the etching rate down. Similarly to before, it can be seen from Fig. 4b that changing the gas flows and concentrations have little effect on the etching rate of the Ni masking layer, which again proves that nickel is a good mask material in this experiment. The reason is that the Ni etching mechanism is dominantly physically bombardment, which is almost insensitive to the gas flow rates. Figure 4c shows the effect of different SF<sub>6</sub>/O<sub>2</sub> gas ratios on the etching rate. It is seen that as the content of O<sub>2</sub> is increased, the etching rate of the substrate first rises and then decreases. That is because, some O can combine with S element in the gas mixture and generate volatile species such as SO↑ and SO<sub>2</sub>↑ [10, 17]. As shown in Eq. (1), this shifts the chemical equilibrium towards the right and thereby increases the concentration of F that can etch Si. When the O<sub>2</sub> concentration is too high, nevertheless, the silicon

substrate oxidation process is enhanced and the etching rate is decreased [10, 18]. Again, altering the  $O_2$  flow has little influence on the Ni masking layer. The results show that the etching rate is the highest when 50 sccm  $O_2$  is introduced, which can be regarded as an optimal DRIE condition.

### 3.4 Effect of different initial etched depth on the etching rate

DRIE deals with deep holes, where the profile of the holes plays a role in the etching kinetics because the plasma etching is in the so-called internal diffusion control regime. That is, the diffusion rates of the reactants and products are the limiting factors of the etching speed. To study this effect, in the following experiment, the structures are etched in separate steps. For each group of experiments, five samples are loaded to the machine altogether. After every 5 min, the chamber is opened and a sample is unloaded, where the etched depth for this specific run is recorded (i.e. the etched

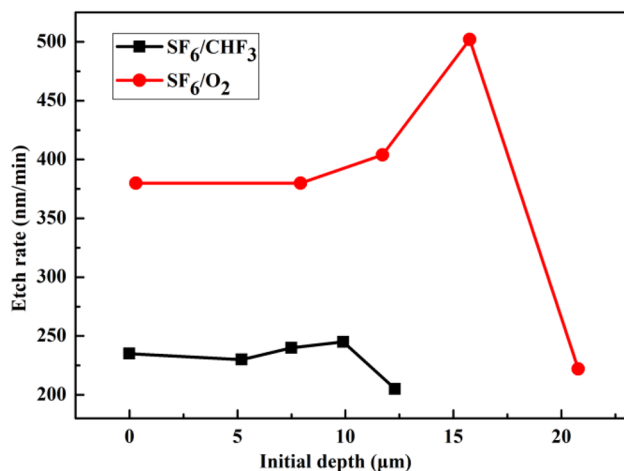
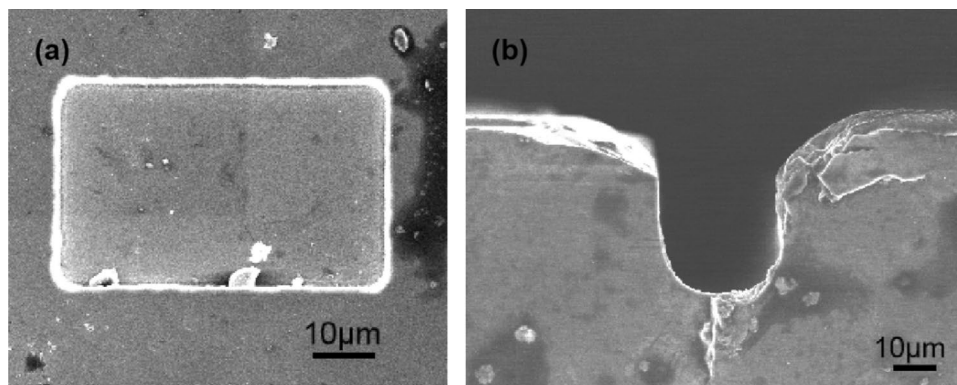


**Fig. 5** Etching rate diagram which is plotted against different initial etching depths (the black block curve is the  $SF_6/CHF_3$  gas mixture etching rate and the red circle curve is the etching curve of the  $SF_6/O_2$  gas mixture)

**Fig. 6** **a** SEM image of the top view of a hole that is 30  $\mu m$  wide and 45  $\mu m$  deep; **b** SEM image of the cross section of the same hole



depths for the earlier runs are subtracted when calculating the etch rate) and plotted in Fig. 5. The sum of the depths of all the prior etching steps is referred to as the initial etched depth and its influence on the present etching step is investigated. The  $SF_6/CHF_3$  (80/50 sccm) gas mixture and the  $SF_6/O_2$  (80/50 sccm) gas mixture have been used as the processing gases. The RF power is maintained at 500 W.

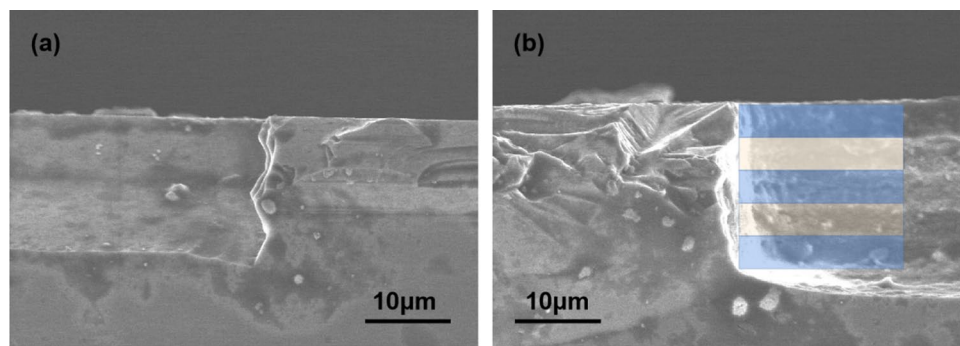
It can be seen from Fig. 5 that for both curves, the etch rate first increases, and when the initial etching depth reaches a certain level, the etch rate will then decrease. This effect can be understood as follows. For each step, when the etching starts, if there already exist some pits in the surface, they serve as microcavities that help to hold the reactants and boost the etching of the silicon in those pits. However, when they become too deep, it is hard for the gaseous chemical products to be transported to the exterior world, which enlarges the scattering, hinders the etching at the trench bottom and slows it down [18]. Interestingly, in Fig. 5, the initial depth dependence of the etching rate is different for different gas mixtures. For the case of  $SF_6/O_2$ , as shown in earlier discussions, the etching rate is generally much faster than that of  $SF_6/CHF_3$ . Here, the etching kinetics is also much more dependent on the profile of the holes.

### 3.5 Microstructure characterization and analysis

Hereby we show some typical micrographs demonstrating that the DRIE of silicon can indeed be achieved by our method. The test structure used in this experiment is a  $30 \times 50 \mu m^2$  hole. The optimized experimental condition obtained above is applied, where a mixed gas flow rate of  $SF_6:O_2 = 80:50$  sccm is used, and the RF power is 500 W. The structure is observed by SEM SU8000 produced by Hitachi.

Figure 6a shows the observation (top view) of an etched hole. The structure is seen to be very clear and neat. Figure 6b is a cross-sectional SEM image of the best result we have obtained so far, which is an etched hole that is as deep as 45  $\mu m$ . That hole is about 30  $\mu m$  wide. The sidewalls of

**Fig. 7** Cross-sectional SEM images of the silicon substrates etched in consecutive steps (10 min for each step). **a** Results of two steps of etching; **b** results of five steps of etching, where the five “layers” are indicated by the color bars and the perpendicularity of the sidewall after five steps of etching



the hole are seen to be rather smooth. In our process, some degrees of sidewall passivation have been achieved by forming  $\text{Si}_x\text{O}_y\text{F}_z$  films with the addition of  $\text{O}_2$  to the  $\text{SF}_6$  plasma [19, 20], which is beneficial for obtaining high aspect ratio.

If no  $\text{O}_2$  is added to the gas mixture, due to the lack of passivation effect of the sidewalls, the cross-sectional profile of the holes can be not that vertical. In this case, we have found that a multi-step etching can compensate this effect to a large extent. A series of experiments are carried out with several consecutive etchings of 10 min in 80 sccm  $\text{SF}_6$  flow. The results are shown in Fig. 7. Figure 7a shows the side profile of a two-step-etched hole observed by SEM. It can be seen that there are two “arcs” at the sidewall. When the number of etch steps is increased to five, the topographical image is shown in Fig. 7b, where the 5 “layers” are marked with different colors. Clearly, these layers on the sidewall are a result of the stepwise etching of the Si. The sidewall is now much more perpendicular, as shown in the image in Fig. 7b. We note that the arc-shaped sidewall is a result of the random scattering of the reactant particles, which etch the sidewalls. Ideally, the incident particles are with relatively high energies, which travel towards the horizontal surface and etch it. However, as the pit gets deeper, the emitted particles of the chemical products as well as the relatively rough nature of the etched pit bottom together lead to the random scattering of the reactant particles [18]. This effect can be reduced by the stepwise etching, because when the gaseous chemicals are pumped out and new gases are introduced into the chamber, the plasma particle incident condition is reset, and the random collisions between the reactant and product particles are decreased. Therefore, the shorter each etch step is, the higher the verticality we can achieve.

## 4 Conclusions

In this paper, we have used a simple structured machine with no ICP sources and no cryogenic units to achieve the purpose of DRIE of silicon that is traditionally accomplished via the Bosch technique [20–24]. By systematically optimizing the parameters of the etching process, we can achieve

a reasonably fast Si etching using  $\text{SF}_6$  and  $\text{O}_2$  plasma. A 45  $\mu\text{m}$  deep Si trench is etched with rather good perpendicularity. Our results are comparable with those of some mainstream technologies [25–27]. This research is of significance to applications that put more requirements on cheaper and simpler equipment and process rather than on extremely high precision of the final products. Some key conclusions are specifically listed below for clarity.

1. As the RF power increases, the etching rate of Si increases. The maximal selectivity between Si and Ni can be about 49:1 at 500 W.
2. Different etching gases have different etching rates on Si but have little effect on the etching of the masking layer. When the ratio of  $\text{SF}_6/\text{O}_2$  is 80/50 sccm, the etching rate reaches  $\sim 440$  nm/min.
3. Initial etched depths have an effect on the etching rate, which is explained by the etching kinetics that is gas composition dependent.

**Acknowledgements** We thank National Natural Science Foundation of China (11674016) and National Key R&D Program of China (2018YFA0209004, 2017YFB0403102) for their financial supports.

## References

1. J.P. Booth, G. Cunge, P. Chabert et al., *J. Appl. Phys.* **85**, 3097–3107 (1999). <https://doi.org/10.1063/1.369649>
2. F. Marty, L. Rousseau, B. Saadany et al., *Microelectron. J.* **36**, 673–677 (2005). <https://doi.org/10.1016/j.mejo.2005.04.039>
3. F. Laermer, A. Urban, *Microelectron. Eng.* **67–68**, 349–355 (2003). [https://doi.org/10.1016/S0167-9317\(03\)00089-3](https://doi.org/10.1016/S0167-9317(03)00089-3)
4. D.G. Choi, H.K. Yu, S.G. Jang et al., *J. Am. Chem. Soc.* **126**, 7019–7025 (2004). <https://doi.org/10.1021/ja0319083>
5. C.M. Waits, B. Morgan, M. Kastantin et al., *Sens. Actuators A Phys.* **119**, 245–253 (2005). <https://doi.org/10.1016/j.sna.2004.03.024>
6. J.W. Bartha, J. Greschner, M. Puech et al., *Microelectron. Eng.* **27**, 453–456 (1995). [https://doi.org/10.1016/0167-9317\(94\)00144-J](https://doi.org/10.1016/0167-9317(94)00144-J)
7. Ü. Sökmen, A. Stranz, S. Fündling et al., *Microsyst Technol.* **16**, 863–870 (2010). <https://doi.org/10.1007/s00542-010-1035-7>
8. T. Sun, J. Miao, H. Zhu et al., *Int. J. Comput. Eng. Sci.* **04**, 319–322 (2003). <https://doi.org/10.1142/S1465876303001174>

9. D. Humbird, D.B. Graves, *Plasma Sour. Sci. Technol.* **11**, A191–A195 (2002). <https://doi.org/10.1088/0963-0252/11/3A/328>
10. H. Jansen, H. Gardeniers, M. Boer et al., *J. Micromech. Microeng.* **6**, 14–28 (1996). <https://doi.org/10.1088/0960-1317/6/1/002>
11. F. Becker, I.W. Rangelow, R. Kassing, *J. Appl. Phys.* **80**, 56–65 (1996). <https://doi.org/10.1063/1.362761>
12. F.H. Bell, O. Joubert, G.S. Oehrlein et al., *J. Vac. Sci. Technol. A Vac. Surf Films* **12**, 3095–3101 (1994). <https://doi.org/10.1116/1.578942>
13. T. Otto, H. Wolf, R. Streiter et al., *Microelectron. Eng.* **45**, 377–391 (1999). [https://doi.org/10.1016/S0167-9317\(98\)00287-1](https://doi.org/10.1016/S0167-9317(98)00287-1)
14. L. Sun, H. Jin, X. Ye et al., *Optik*. **127**, 206–211 (2016). <https://doi.org/10.1016/j.ijleo.2015.10.046>
15. H.V. Jansen, J.G.E. Gardeniers, J. Elders et al., *Sens. Actuators A Phys.* **41**, 136–140 (1994). [https://doi.org/10.1016/0924-4247\(94\)80101-0](https://doi.org/10.1016/0924-4247(94)80101-0)
16. E. Gogolides, S. Grigoropoulos, A.G. Nassiopoulou, *Microelectron. Eng.* **27**, 449–452 (1995). [https://doi.org/10.1016/0167-9317\(94\)00143-1](https://doi.org/10.1016/0167-9317(94)00143-1)
17. R. D'Agostino, D.L. Flamm, *J. Appl. Phys.* **52**, 162–167 (1981). <https://doi.org/10.1063/1.328468>
18. C.P. Demic, K.K. Chan, J. Blum, *J. Vac. Sci. Technol. B* **10**, 1105–1110 (1992). <https://doi.org/10.1116/1.586085>
19. A.K. Paul, A.K. Dimri, R.P. Bajpai, *Vacuum* **68**, 191–196 (2002). [https://doi.org/10.1016/S0042-207X\(02\)00387-1](https://doi.org/10.1016/S0042-207X(02)00387-1)
20. H. Jansen, M. Boer, R. Legtenberg et al., *J. Micromech. Microeng.* **5**, 115–120 (1995). <https://doi.org/10.1088/0960-1317/5/2/015>
21. X. Wang, Y. Chen, L. Wang et al., *Microelectron. Eng.* **85**, 1015–1017 (2008). <https://doi.org/10.1016/j.mee.2008.01.073>
22. M.K. Hooda, M. Wadhwa, S. Verma et al., *Vacuum* **84**, 1142–1148 (2010). <https://doi.org/10.1016/j.vacuum.2010.01.052>
23. E.H. Klaassen, K. Petersen, J.M. Noworolski et al., *Sens. Actuators A Phys.* **52**, 132–139 (1996). [https://doi.org/10.1016/0924-4247\(96\)80138-5](https://doi.org/10.1016/0924-4247(96)80138-5)
24. P.T. Docker, P.K. Kinnell, M.C.L. Ward, *J. Micromech. Microeng.* **14**, 941–944 (2004). <https://doi.org/10.1088/0960-1317/14/7/014>
25. J. Ohara, Y. Takeuchi, K. Sato, *J. Micromech. Microeng.* **19**, 0950022 (2009). <https://doi.org/10.1088/0960-1317/19/9/095022>
26. K. Ishihara, Y. Chi-Fan, A.A. Ayon et al., *J. Microelectromech. Syst.* **8**, 403–408 (1999). <https://doi.org/10.1109/84.809054>
27. W.-S. Kim, W. Lee, H.-W. Cheong et al., *J. Korean Phys. Soc.* **65**, 1399–1403 (2014). <https://doi.org/10.3938/jkps.65.1399>

**Publisher's Note** Springer Nature remains neutral with regard to jurisdictional claims in published maps and institutional affiliations.